J. Fluid Mech. (1996), vol. 327, pp. 255–272

The transverse shear-induced liquid and particle tracer diffusivities of a dilute suspension of spheres undergoing a simple shear flow

By Y. WANG[1], R. MAURI[2] AND A. ACRIVOS[1]

[1] Levich Institute, T-1M, City College of CUNY, New York, NY 10031, USA

[2] Department of Chemical Engineering, City College of CUNY, New York, NY 10031, USA

(Received 21 March 1994 and in revised form 21 June 1996)

We study the shear-induced self-diffusion of both a liquid tracer and a tagged spherical particle along the directions perpendicular to the ambient flow in a dilute suspension of neutrally buoyant spheres undergoing a simple shearing motion in the absence of inertia and Brownian motion effects. The calculation of the liquid diffusivity requires the velocity of a fluid point under the influence of two spheres, which was determined via Lamb's series expansion; conversely, the calculation of the particle diffusivity involves the trajectories of three spheres, which were determined using far-field and near-field asymptotic expressions. The displacements of the liquid tracer and of the tagged sphere were then computed analytically when the spheres and the tracer are all far apart, and numerically for close encounters. After summing over all possible encounters, the leading terms of the lateral liquid diffusion coefficients, both within and normal to the plane of shear, were thereby found to be $0.12\gamma a^2c^2$ and $0.004\gamma a^2c^2$, respectively, where γ is the applied shear rate, a the radius of the spheres and c their volume fraction. The analogous coefficients of the lateral particle diffusivity were found to be $0.11\gamma a^2c^2$ and $0.005\gamma a^2c^2$, respectively. Also, liquid and particle diffusivities in a monolayer, with the liquid tracer and all the particle centres lying on the same plane of shear, were found to be $0.067\gamma a^2\bar{c}^2$ and $0.032\gamma a^2\bar{c}^2$, respectively, with $\bar{c}$ denoting the areal fraction occupied by the spheres on the plane.

1. Introduction

The non-Brownian particle migration in suspensions involving only deterministic hydrodynamic interactions can often be represented in terms of a self-diffusion process owing to the random nature of the collisions among the suspended particles. Such a shear-induced particle diffusion has been shown to play an important role in a variety of phenomena involving concentrated suspensions which affect certain of their properties in a profound way. Shear-induced diffusion was first studied experimentally by Eckstein, Bailey & Shapiro (1977), who monitored the motion of a tagged particle within a suspension being sheared in a Couette device, and then was examined in more detail by Leighton & Acrivos (1987*a*, *b*) who reported experimental values for the lateral diffusion coefficients both within and normal to the plane of shear. Two-dimensional numerical simulations by Bossis & Brady (1987) and by Chang & Powell (1994) for the monolayer diffusivity were found to agree qualitatively with these results. Recently, by considering only two-particle interactions, Acrivos *et al.* (1992) derived an analytic expression for the coefficient of shear-induced self-diffusion

in the direction of the fluid motion for a dilute suspension of spheres undergoing a simple shearing motion, while da Cunha & Hinch (1996) studied the effect of surface roughness on the interaction of two particles and calculated the coefficients of the self- and gradient-diffusivity in the lateral directions. Here, we shall extend the analysis of Acrivos *et al.* (1992) and present expressions for the self-diffusivity of both a tracer fluid particle and a test sphere in the two directions perpendicular to the fluid velocity.

This paper proceeds as follows. After formulating the problem in §2, we derive in §§3 and 4 the expressions for the velocities of the fluid tracer plus those of the test sphere as well as the other two spheres in a simple shear flow, which are then used in §5 to compute the displacement of a liquid tracer and of a test sphere following their encounter with the other two particles. Finally, in §6, we determine the coefficients of self-diffusion in the directions perpendicular to the fluid velocity, both within and normal to the plane of shear.

2. Statement of the problem

Consider a dilute monodisperse suspension of rigid spheres of radius a immersed in a viscous liquid. The spheres are supposed to be neutrally buoyant and torque-free, and their radius a is taken to be sufficiently large that the effects of Brownian motion and interparticle potentials can be neglected. Furthermore, the particle Reynolds number is assumed to be vanishingly small, so that all inertia effects can be ignored. Now, let the suspension undergo a simple shearing motion, the undisturbed velocity of which is given by

$$\boldsymbol{U} = x_2 \boldsymbol{e}_1, \tag{1}$$

where (x_1, x_2, x_3) is the position vector relative to a fixed triad of unit vectors $\boldsymbol{e}_1$, $\boldsymbol{e}_2$ and $\boldsymbol{e}_3$ which forms a right-hand system. All lengths, time and velocities are regarded as having been non-dimensionalized with a, $1/\gamma$ and γa respectively, where γ is the shear rate.

First, consider a fluid point A* and let $\boldsymbol{X}$ denote its position, where $\boldsymbol{X} = 0$ initially. In the absence of the suspended spheres, A* would simply remain at the origin. However, when a sphere B, with its centre located at $\boldsymbol{Y}$, approaches from far away, A* will be displaced at first from the origin, but will return to its initial streamline at the end of the encounter, as a consequence of the reversibility of the creeping flow equations and the symmetry of the problem. Hence, the interaction of a fluid tracer with a single sphere will not lead to its being permanently displaced in the lateral direction, and therefore to create such a displacement, it is necessary that A* and B interact with at least another sphere C located at $\boldsymbol{Z}$ (see figure 1).

Since the probability of finding two spheres within an $O(1)$ distance from the tracer is $O(c^2)$, where c is the particle volume fraction, we expect the rate of encounters of a fluid tracer with two spheres to be of $O(c^2)$. In addition, as the rate of encounters involving more spheres is of $o(c^2)$, we need to consider only the interactions of the tracer with two spheres in order to calculate the leading-order term of the lateral diffusivities of the fluid tracer.

As a result of its encounters with the other two spheres, the fluid tracer in a statistically homogeneous suspension suffers a series of random displacement with zero mean. In a dilute suspension, these encounters can be regarded as statistically independent and thus the displacement of the fluid tracer in the lateral direction can be treated as a self-diffusive process with the diffusion coefficients D_2^* and D_3^* being

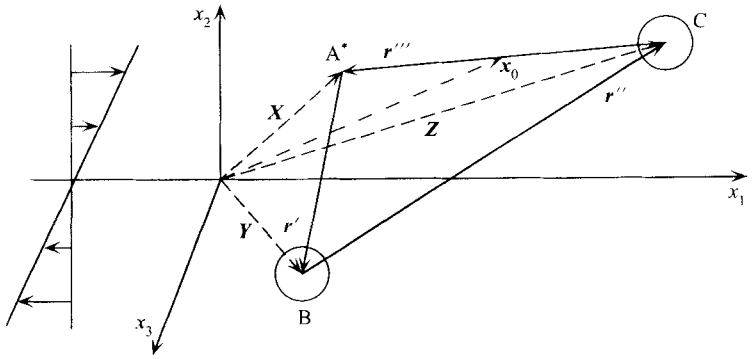

FIGURE 1. Coordinates used in this work.

defined as

$$D_j^* \equiv \lim_{T\to\infty} \frac{1}{2T} \sum_{k=1}^{N} (\Delta X_j^{(k)})^2, \tag{2}$$

where $\Delta X_j^{(k)}$ refers to the displacement of the fluid tracer in the j-direction ($j = 2, 3$) resulting from its kth encounter with two spheres and N is the total number of such encounters within the time interval T.

Obviously, both the values of $\Delta X_j^{(k)}$ and the rate of encounters are determined by the initial positions of the two spheres, once the probability distribution of the initial configurations is known. Thus, as shown below, for statistically homogeneous suspensions at steady state, the expression for D_j^* given above can be reduced to an integral of the contributions over all the possible initial positions of the two spheres, which is more convenient to evaluate than the summation in (2).

Before analysing the different types of possible initial configurations of the spheres, we note that, in order for an encounter to create a significant permanent lateral displacement $\Delta X_j^{(k)}$, the fluid tracer and the two spheres must all be reasonably close to each other during a certain period of time. Otherwise, the fluid tracer will interact separately with the two spheres and therefore will not suffer a permanent lateral displacement. Thus, we consider only those initial configurations where, at some time during their encounter, the spheres and the fluid tracer happen to lie within a cubic 'collision box' of dimensions $(2l)^3$. Later on, we shall show that the contribution to D_j^* in (2) due to the encounters which take place outside the collision box (i.e. such that the fluid tracer and the two spheres are never present within the collision box at the same time) tends to zero as $l \longrightarrow \infty$. Therefore, the integration over the initial configurations tends to a constant value that can be determined numerically, without the need to introduce a renormalization as often happens with other calculations involving the effective properties of suspensions.

Now, prior to the encounter, the initial positions of spheres B and C will belong to one of the following three categories:

(i) both spheres B and C are far away from the fluid tracer;

(ii) the fluid tracer A* orbits around one of the spheres as long as the other sphere is far away;

(iii) the fluid tracer A* together with the spheres B and C form a permanent triplet.

First, consider case (i), where initially the fluid tracer A* is located at the origin while spheres B and C can be either on the left or on the right side of the collision box. But, by virtue of the symmetry of the particle distribution about the origin, we

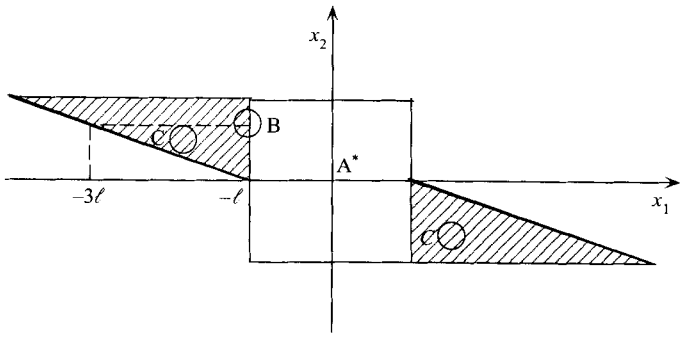

FIGURE 2. The integration domains W_0^B and W_0^C, within the plane $x_3 = 0$.

only need to consider the case where the sphere B, chosen as the sphere which first crosses the boundary of the box, enters from the left side at $t = 0$.

Now, when we calculate the contribution of this case to the diffusion coefficient in (2), we consider all possible initial positions of spheres B and C, such that A*, B and C find themselves inside the collision box at some stage during the course of their encounter. The loci of these initial positions of B and C form two domains W^B and W^C, which can be determined by first neglecting the interactions among the spheres, so that B and C can be assumed to move with the velocity of the ambient flow. Then, obviously, $\boldsymbol{Y}^{(0)}$, which refers to the initial position of B, can only lie on the upper half of the left-hand surface of the box. We denote this domain by W_0^B: $\{-l \leqslant Y_3^{(0)} \leqslant l,\ \ 0 \leqslant Y_2^{(0)} \leqslant l\}$. Accordingly, since B stays inside the box from $t = 0$ to $t = 2l/Y_2^{(0)}$, the possible initial position of C, $\boldsymbol{Z}^{(0)}$, must lie within that part of the fluid which flows into the box during that period of time. This domain W_0^C has the shape of two wedges, one of which is given by $\{-l \leqslant Z_3^{(0)} \leqslant l,\ \ 0 \leqslant Z_2^{(0)} \leqslant l,\ \ -l - 2lZ_2^{(0)}/Y_2^{(0)} \leqslant Z_1^{(0)} \leqslant -l\}$ while the other is that generated by rotating the wedge depicted above about the axis x_3 by an angle π (see figure 2).

In arriving at the above estimate, all hydrodynamic interactions among the spheres and the fluid tracer were neglected, but obviously these interactions will alter the domains only slightly. First of all, the time needed for sphere B to pass through the collision box will be slightly different from that estimated above by an amount that can be evaluated exactly through a direct numerical calculation of its trajectory. Secondly, when the interactions between B and C are considered, one needs to take into account the possibility that, initially, B could be located on the lower half of the left-hand surface of the collision box, i.e. even when $Y_2^{(0)} < 0$, B could still end up moving from left to right in certain cases. This happens, for example, when B and C form a permanent doublet when left alone in the ambient flow, provided that the midpoint between B and C lies above the plane $x_2 = 0$. The real domain W^B is therefore slightly larger than the estimate W_0^B and its exact shape can be determined via the solution of the pair sphere trajectories (Batchelor & Green 1972*a*). These considerations can be extended to W^C.

Next, we consider the rate at which a pair of spheres B and C enters the collision box, with B initially lying in the surface element $\mathrm{d}Y_2^{(0)}\mathrm{d}Y_3^{(0)}$ and C within the volume element $\mathrm{d}Z_1^{(0)}\mathrm{d}Z_2^{(0)}\mathrm{d}Z_3^{(0)}$. Now, the rate at which B enters the box is given by $nV_1^B\mathrm{d}Y_2^{(0)}\mathrm{d}Y_3^{(0)}|_{Y_1^{(0)}=-l}$, with n denoting the number of spheres per unit volume and

V_1^B the velocity of B along the e_1-direction, while the probability of finding C within the volume element $dZ_1^{(0)}dZ_2^{(0)}dZ_3^{(0)}$ inside the domain W^C is $np(\boldsymbol{r}_{BC})dZ_1^{(0)}dZ_2^{(0)}dZ_3^{(0)}$, where $p(\boldsymbol{r}_{BC})$ is the pair distribution function. When only two-sphere interactions are considered, $p(\boldsymbol{r})$ equals the function $q(r)$ of Batchelor & Green (1972*b*) if $\boldsymbol{r}$ lies outside the region of closed trajectories, and is indeterminate when it lies inside. In §6, we shall show that our final results are very insensitive to the specific form of $p(\boldsymbol{r})$ which is assumed to apply in the region of closed trajectories.

Finally, the contribution of case (i) to the sum in (2) is given by

$$D_j^{*'} = n^2 \int_{W^B} \int_{W^C} p(\boldsymbol{r}_{BC})(\Delta X_j)^2 V_1^{(B)} dY_2^{(0)} dY_3^{(0)} dZ_1^{(0)} dZ_2^{(0)} dZ_3^{(0)}, \tag{3}$$

where ΔX_j is the net displacement of A* resulting from its encounter with B and C initially lying within the elements $dY_2^{(0)}dY_3^{(0)}$ and $dZ_1^{(0)}dZ_2^{(0)}dZ_3^{(0)}$, respectively.

For case (ii), we label as C the sphere around which A* would orbit indefinitely in the absence of another particle. Now, in most cases C will be close to A*, so that, for large enough l, we can take $p(\boldsymbol{r}_{BC}) = 1$. The contribution of case (ii) to the sum (2) is then given by

$$D_j^{*''} = n^2 \int_{W_0^B} \int_{A^*,C \text{ bound}} (\Delta X_j)^2 V_1^{(B)} dY_2^{(0)} dY_3^{(0)} dZ_1^{(0)} dZ_2^{(0)} dZ_3^{(0)}. \tag{4}$$

Here though, before the encounter, X_j changes periodically with time and its average value equals that of the position of the centre of C. Moreover, since for dilute suspensions, B is located initially very far from the pair, the net displacement of A* occurs on a time scale much larger than that required for the pair to complete one revolution. In addition, we note that the periodic motion of the tracer particle A* around C does not, by itself, contribute to the diffusion process. Hence, to be consistent with (2), and given that the initial location of B is also random, we take this average value of A* orbiting about C before the encounter as the initial position of A*. After the encounter, the initially bound A* can either continue orbiting around C or be displaced out of the region of closed trajectories. In the former case, we take the average value of X_j, which is the same as the position of the centre of the sphere around which it orbits, as the final position of A*. Now, as any two-sphere interactions do not lead to a permanent lateral displacement of the spheres, the net displacement of A* in this case will be zero. So, the only possible contribution to $D_j^{*''}$ comes from those cases for which A* is displaced out of the region of closed trajectories around C.

Finally, for case (iii), where A*, B and C form a permanent triplet, the net lateral displacement of A* is zero as a consequence of the reversibility of the creeping flow equations and the symmetry of the ambient flow. Therefore this case does not contribute to the sum (2), so that we obtain

$$D_j^* = D_j^{*'} + D_j^{*''}. \tag{5}$$

In the same way, we can also define a monolayer diffusivity by assuming that the fluid tracer together with the centres of the other two spheres are confined on the same plane of shear. Obviously, all the trajectories of the fluid tracer and the particle centres will remain on that plane, owing to symmetry. In this case, the diffusivity of the tracer is given by

$$\bar{D}_2^* = \bar{D}_2^{*'} + \bar{D}_2^{*''}, \tag{6}$$

with

$$\bar{D}_2^{*\prime} = \bar{n}^2 \int_{\bar{W}^B} \int_{\bar{W}^C} \bar{p}(r_{BC})(\Delta \bar{X}_2)^2 V_1^{(B)} \mathrm{d}Z_1^{(0)} \mathrm{d}Z_2^{(0)} \mathrm{d}Y_2^{(0)} \tag{7}$$

and

$$\bar{D}_2^{*\prime\prime} = \bar{n}^2 \int_{\bar{W}^B} \int_{A^*,C \text{ bound}} (\Delta \bar{X}_2)^2 V_1^{(B)} \mathrm{d}Z_1^{(0)} \mathrm{d}Z_2^{(0)} \mathrm{d}Y_2^{(0)}. \tag{8}$$

Here $\bar{n}$ denotes the number of spheres per unit area on the plane, and

$$\bar{p}(r) = \frac{1}{1-A} \exp \int_r^\infty \frac{2(B-A)}{r(1-A)} \mathrm{d}r$$

is the probability density for a monolayer of particles, as obtained by adapting to the two-dimensional case Batchelor & Green's (1972*b*) analysis for $p(r)$, with the functions $A(r)$ and $B(r)$ given by Batchelor & Green (1972*a*).

Similar expressions for the self-diffusivity D_j and the monolayer self-diffusivity $\bar{D}_2$ of a test sphere A can be written, with the fluid tracer A* replaced by the test sphere A. It should be noted though that, in computing the contribution to D_j'' for bound pairs, cf. (4), account should be taken of the fact that, as a result of its interaction with particle B, the doublet A-C will now suffer a net lateral displacement in contrast to the case when A is replaced by the fluid point A*.

3. The velocity of a fluid tracer in the presence of two spheres

Since the liquid tracer diffusivity depends on the lateral displacement of the fluid tracer for any given initial positions of the spheres B and C at time $t = 0$ (see (2)), we need to obtain the fluid velocity field in the vicinity of two spheres undergoing a simple shear flow, together with the velocities of the two spheres themselves. Now, while the latter are given in Batchelor & Green (1972*a*), the fluid velocity can be determined through a far-field expansion when the fluid point and the spheres are all far apart, and by Lamb's series expansion when they are close together.

The far-field expression of the fluid velocity was determined using the method of reflections, which we carried out up to and including terms of $O(1/\bar{r}^7)$, with $\bar{r}$ denoting the typical distance between the two spheres or that between the liquid tracer and one of the spheres. Therefore, the velocity of A* can be written as

$$\boldsymbol{V}^{(A^*)} = \boldsymbol{U}(\boldsymbol{X}) + \boldsymbol{V}_{B\to A^*} + \boldsymbol{V}_{C\to A^*} + \boldsymbol{V}_{B\to C\to A^*} + \boldsymbol{V}_{C\to B\to A^*} + O\left(1/\bar{r}^8\right), \tag{9}$$

where the subscripts denote the sequences of reflections. A direct calculation yields the following explicit expression:

$$\begin{aligned}
\boldsymbol{V}^{(A^*)} = \boldsymbol{U}(\boldsymbol{X}) &+ \boldsymbol{r}' \cdot \boldsymbol{E} \cdot [A^*(r')\boldsymbol{r}'\boldsymbol{r}'/r'^2 + B^*(r')(\boldsymbol{I} - \boldsymbol{r}'\boldsymbol{r}'/r'^2)] \\
&- \boldsymbol{r}''' \cdot \boldsymbol{E} \cdot [A^*(r''')\boldsymbol{r}'''\boldsymbol{r}'''/r'''^2 + B^*(r''')(\boldsymbol{I} - \boldsymbol{r}'''\boldsymbol{r}'''/r'''^2)] \\
&+ \tfrac{1}{2}\boldsymbol{F}(\boldsymbol{r}''') : \{\nabla \boldsymbol{F}(\boldsymbol{r}'') : \boldsymbol{E} + [\nabla \boldsymbol{F}(\boldsymbol{r}'') : \boldsymbol{E}]^T\} \\
&+ \tfrac{1}{20}\boldsymbol{F}(\boldsymbol{r}''') : \nabla^2\{\nabla \boldsymbol{F}(\boldsymbol{r}'') : \boldsymbol{E} + [\nabla \boldsymbol{F}(\boldsymbol{r}'') : \boldsymbol{E}]^T\} \\
&+ \tfrac{7}{24}(\boldsymbol{r}'''\nabla\nabla\nabla(1/r''')) : \boldsymbol{G}(\boldsymbol{r}'') - \tfrac{1}{8}\nabla\nabla(1/r''') : \boldsymbol{G}(\boldsymbol{r}'') \\
&+ \tfrac{5}{12}\boldsymbol{G}(\boldsymbol{r}'') : (\nabla\nabla(1/r''')) - \tfrac{1}{12}(\nabla\nabla(1/r''')) \cdot [\boldsymbol{I} : \boldsymbol{G}(\boldsymbol{r}'')] \\
&- \tfrac{1}{2}\boldsymbol{F}(\boldsymbol{r}') : \{\nabla \boldsymbol{F}(\boldsymbol{r}'') : \boldsymbol{E} + [\nabla \boldsymbol{F}(\boldsymbol{r}'') : \boldsymbol{E}]^T\} \\
&- \tfrac{1}{20}\boldsymbol{F}(\boldsymbol{r}') : \nabla^2\{\nabla \boldsymbol{F}(\boldsymbol{r}'') : \boldsymbol{E} + [\nabla \boldsymbol{F}(\boldsymbol{r}'') : \boldsymbol{E}]^T\}
\end{aligned}$$

$$-\tfrac{7}{24}(\boldsymbol{r}'\nabla\nabla\nabla(1/r')):\boldsymbol{G}(\boldsymbol{r}'') + \tfrac{1}{8}\nabla\nabla(1/r') : \boldsymbol{G}(\boldsymbol{r}'')$$
$$-\tfrac{5}{12}\boldsymbol{G}(\boldsymbol{r}'') : (\nabla\nabla(1/r')) + \tfrac{1}{12}(\nabla\nabla(1/r'))\cdot[\boldsymbol{I} : \boldsymbol{G}(\boldsymbol{r}'')] + O(1/\bar{r}^8), \qquad (10)$$

where $\boldsymbol{r}' = \boldsymbol{Y} - \boldsymbol{X}$, $\boldsymbol{r}'' = \boldsymbol{Z} - \boldsymbol{Y}$ and $\boldsymbol{r}''' = \boldsymbol{X} - \boldsymbol{Z}$ are the particle relative position vectors, $\boldsymbol{E} = (\boldsymbol{e}_1\boldsymbol{e}_2 + \boldsymbol{e}_2\boldsymbol{e}_1)/2$ is the rate-of-strain tensor of the ambient flow, while $A^*(r)$ and $B^*(r)$ are the scalar functions:

$$A^*(r) = \frac{5}{2r^3} - \frac{3}{2r^5}, \quad B^*(r) = \frac{1}{r^5}, \qquad (11)$$

and the functions $\boldsymbol{F}(\boldsymbol{r})$ and $\boldsymbol{G}(\boldsymbol{r})$ are the third-order tensors

$$\boldsymbol{F}(\boldsymbol{r}) = -\frac{5}{6}\boldsymbol{r}\nabla\nabla\frac{1}{r} - \frac{1}{6}\nabla\nabla\nabla\frac{1}{r}, \quad \boldsymbol{G}(\boldsymbol{r}) = \frac{1}{2}\nabla\nabla\boldsymbol{F}(\boldsymbol{r}) : \boldsymbol{E}. \qquad (12)$$

When A*, B and C are not all far apart, we used Lamb's series expansion to determine the velocity of the liquid tracer together with the results of Yoon & Kim (1987), who determined the strengths of the singularities (i.e. the coefficients in Lamb's expression) at the centre of two spheres moving in pure straining fluid flows. From these coefficients we constructed a general expression for the fluid velocity, noting that the motion of a fluid point near two arbitrarily oriented spheres in a simple shear flow can be decomposed into a uniform translation, a rigid-body rotation and a pure straining flow with rate of strain tensor $\boldsymbol{E} = (\boldsymbol{e}_1\boldsymbol{e}_2 + \boldsymbol{e}_2\boldsymbol{e}_1)/2$. Now, the contributions from the first two parts are obvious and that from the third part is determined by transforming the old reference frame into a new one, say O', in such a way that the centres of B and C lie on the $\boldsymbol{e}_3'$-axis and are symmetric with respect to the new origin, with $\boldsymbol{e}_2' = \boldsymbol{e}_3 \times \boldsymbol{e}_3'/|\boldsymbol{e}_3 \times \boldsymbol{e}_3'|$, and $\boldsymbol{e}_1' = \boldsymbol{e}_2' \times \boldsymbol{e}_3'$.

But, as pointed out by Kim & Karrila (1991), the rate of strain tensor $\boldsymbol{E}$, in the new coordinate frame, can be expressed as a linear combination of $\boldsymbol{E}^{(1)'} = \frac{1}{2}\boldsymbol{e}_1'\boldsymbol{e}_1' + \frac{1}{2}\boldsymbol{e}_2'\boldsymbol{e}_2' - \boldsymbol{e}_3'\boldsymbol{e}_3'$, $\boldsymbol{E}^{(2)'} = \boldsymbol{e}_2'\boldsymbol{e}_3' + \boldsymbol{e}_3'\boldsymbol{e}_2'$, $\boldsymbol{E}^{(3)'} = \boldsymbol{e}_1'\boldsymbol{e}_2' + \boldsymbol{e}_2'\boldsymbol{e}_1'$, $\boldsymbol{E}^{(4)'} = \boldsymbol{e}_1'\boldsymbol{e}_3' + \boldsymbol{e}_3'\boldsymbol{e}_1'$, and $\boldsymbol{E}^{(5)'} = \boldsymbol{e}_1'\boldsymbol{e}_1' - \boldsymbol{e}_2'\boldsymbol{e}_2'$ (This decomposition is consistent with the fact that any traceless rate of strain tensor has five independent components.) So, our problem reduces to that of determining the fluid velocity $\boldsymbol{v}^{(k)'}$ due to the presence of two spheres in an unperturbed flow field having constant shear rates $\boldsymbol{E}^{(k)'}$, with $k = 1$ to 5. Now, the cases $k = 1$, 2 and 3 are exactly the same as the three subproblems solved by Yoon & Kim (1987), while the last two cases can be easily reduced to the second and third, respectively, by appropriate coordinate transformations, namely $\boldsymbol{v}^{(4)'}(x_1', x_2', x_3') = \boldsymbol{v}^{(2)'}(-x_2', x_1', x_3')$, and $\boldsymbol{v}^{(5)'}(x_1', x_2', x_3') = \boldsymbol{v}^{(3)'}((1/\sqrt{2})(x_1' - x_2'), (1/\sqrt{2})(x_1' + x_2'), x_3')$.

Thus, by combining all these contributions, we found a series expression for the velocity of the liquid tracer for any given position of the fluid tracer and of the spheres B and C. Unfortunately, this series expansion converges very slowly when the spheres are close to each other ($r_{BC} - 2 < 0.01$) and the fluid tracer is close to the surface of one of the spheres or to both of them. Therefore, since during their motion the two spheres can get very close to each other, special care must be taken for these cases.

First, we noted that in order to keep the computation time within reasonable limits, we had to truncate Lamb's expansion after 100 terms. In this case, the truncated series begins to lose its accuracy at distances smaller than 0.01 from the particle surface. Moreover, when the fluid point was placed on the particle surface, its velocity relative to that of the surface, as computed by the series solution, was found to be non-negligible, unless many more terms in Lamb's expansion were retained. This is an important point not only because a small error in the determination of the fluid

velocity field could change significantly the final lateral position of the liquid tracer, but also because it could cause the liquid tracer to penetrate the solid sphere, thereby terminating the computation. But, when the liquid tracer is close to only one of the spheres, the leading term of its tangential and normal velocities relative to those of the surface of the sphere are obviously linear and quadratic in the distance from the surface, respectively. We then determined the corresponding local proportionality coefficients in the expressions for the tangential and normal velocity components referred to above, from the accurate velocity field at a distance 0.01 radii away from the surface, which was calculated via the 100-term Lamb's expansion and the known velocity of the surface of the sphere (Yoon & Kim 1987). Thus, the velocity of any fluid point in this small region could be easily computed accurately to leading order.

Conversely, when the liquid tracer lies in the gap between two almost-touching spheres, we used the lubrication approximation to determine its velocity for the three subproblems corresponding to $\boldsymbol{E}^{(1)'}$, $\boldsymbol{E}^{(2)'}$ and $\boldsymbol{E}^{(3)'}$ defined above. In the first subproblem the two spheres move along their centreline with known opposite velocities (Yoon & Kim 1987) and thus the velocity of the fluid point in the gap is the same as that between two squeezing spheres in a fluid which is at rest at infinity. In the second subproblem, the spheres move normal to their centreline with again known translational and angular velocities, which can be treated separately. The velocity of the fluid point in the gap in these cases can be determined using the velocity expressions in the lubrication approximation. In the third subproblem, the spheres remain stationary and the velocity of the fluid point is negligible, at least to the same order of approximation as in the above two cases. Thus combining the results of the three subproblems, we were able to determine accurately, to leading order in the gap distance, the velocity of the fluid point within the gap separating the two spheres.

In both cases, our approximate fluid velocities were found to differ by less than 0.2% from the results that were obtained using the truncated series expression with more terms retained.

4. The interaction of three spheres

For any set of initial positions of spheres B and C, the lateral displacement ΔX_j of the test sphere A was determined by following the trajectories of A, B and C. This required the evaluation of the velocities of the spheres at a very large number of points, which forced us to use a method that is somewhat simpler than those employed by previous investigators (Mazur & Van Saarloos 1982; Van Saarloos & Mazur 1983; Kim 1987; Hassonjee, Pfeffer & Ganatos 1992; Cichocki *et al.* 1994), specifically the method of reflections when all the spheres are far apart from each other, and an asymptotic expression when two of the spheres are close to each other.

In the first case, the reflections were carried out up to and including terms of $O(1/\bar{r}^7)$, with $\bar{r}$ denoting the typical distance between any two spheres. Therefore, the velocity of A can be written as

$$\begin{aligned} \boldsymbol{V}^{(A)} = \boldsymbol{U}(\boldsymbol{X}) &+ \boldsymbol{V}_{B\to A} + \boldsymbol{V}_{C\to A} + \boldsymbol{V}_{A\to C\to A} + \boldsymbol{V}_{A\to B\to A} \\ &+ \boldsymbol{V}_{B\to C\to A} + \boldsymbol{V}_{C\to B\to A} + O(1/\bar{r}^8). \end{aligned} \tag{13}$$

The velocities of B and C can be obtained from (13) by just shifting the labels. A direct calculation yields the following explicit expression:

$$\begin{aligned} \boldsymbol{V}^{(A)} = \boldsymbol{U}(\boldsymbol{X}) &+ \tfrac{1}{2}\boldsymbol{r}' \cdot \boldsymbol{E} \cdot [A(r')\boldsymbol{r}'\boldsymbol{r}'/r'^2 + B(r')(\boldsymbol{I} - \boldsymbol{r}'\boldsymbol{r}'/r'^2)] \\ &- \tfrac{1}{2}\boldsymbol{r}''' \cdot \boldsymbol{E} \cdot [A(r''')\boldsymbol{r}'''\boldsymbol{r}'''/r'''^2 + B(r''')(\boldsymbol{I} - \boldsymbol{r}'''\boldsymbol{r}'''/r'''^2)] \end{aligned}$$

$$+\tfrac{1}{2}[\boldsymbol{F}(\boldsymbol{r}''')+\tfrac{1}{6}\nabla^2\boldsymbol{F}(\boldsymbol{r}''')]:\{\nabla\boldsymbol{F}(\boldsymbol{r}''):\boldsymbol{E}+[\nabla\boldsymbol{F}(\boldsymbol{r}''):\boldsymbol{E}]^T\}$$
$$+\tfrac{1}{20}\boldsymbol{F}(\boldsymbol{r}'''):\nabla^2\{\nabla\boldsymbol{F}(\boldsymbol{r}''):\boldsymbol{E}+[\nabla\boldsymbol{F}(\boldsymbol{r}''):\boldsymbol{E}]^T\}$$
$$+\tfrac{7}{24}(\boldsymbol{r}'''\nabla\nabla\nabla(1/r''')):\boldsymbol{G}(\boldsymbol{r}'')-\tfrac{1}{8}\nabla\nabla(1/r'''):\boldsymbol{G}(\boldsymbol{r}'')$$
$$+\tfrac{5}{12}\boldsymbol{G}(\boldsymbol{r}''):(\nabla\nabla(1/r'''))-\tfrac{1}{12}(\nabla\nabla(1/r'''))\cdot[\boldsymbol{I}:\boldsymbol{G}(\boldsymbol{r}'')]$$
$$-\tfrac{1}{2}[\boldsymbol{F}(\boldsymbol{r}')+\tfrac{1}{6}\nabla^2\boldsymbol{F}(\boldsymbol{r}')]:\{\nabla\boldsymbol{F}(\boldsymbol{r}''):\boldsymbol{E}+[\nabla\boldsymbol{F}(\boldsymbol{r}''):\boldsymbol{E}]^T\}$$
$$-\tfrac{1}{20}\boldsymbol{F}(\boldsymbol{r}'):\nabla^2\{\nabla\boldsymbol{F}(\boldsymbol{r}''):\boldsymbol{E}+[\nabla\boldsymbol{F}(\boldsymbol{r}''):\boldsymbol{E}]^T\}$$
$$-\tfrac{7}{24}(\boldsymbol{r}'\nabla\nabla\nabla(1/r')):\boldsymbol{G}(\boldsymbol{r}'')+\tfrac{1}{8}\nabla\nabla(1/r'):\boldsymbol{G}(\boldsymbol{r}'')$$
$$-\tfrac{5}{12}\boldsymbol{G}(\boldsymbol{r}''):(\nabla\nabla(1/r'))+\tfrac{1}{12}(\nabla\nabla(1/r'))\cdot[\boldsymbol{I}:\boldsymbol{G}(\boldsymbol{r}'')]+O(1/\bar{r}^8), \tag{14}$$

where the tensors $\boldsymbol{F}$ and $\boldsymbol{G}$ are given by (12) and

$$A(r)=\frac{5}{r^3}-\frac{8}{r^5}+\frac{25}{r^6}-\frac{35}{r^8}+O(1/r^9),\quad B(r)=\frac{16}{3r^5}+\frac{10}{3r^8}+O(1/r^9), \tag{15}$$

from da Cunha & Hinch (1996).

By applying equations (14) and (15) to the case $\boldsymbol{X}=(0,0,0)$, $\boldsymbol{Y}=(2\sqrt{3},0,2)$ and $\boldsymbol{Z}=(2\sqrt{3},2,0)$, we found that the sphere velocities thereby obtained differed from those of the full numerical solution of Hassonjee *et al.* (1992) by less than 0.4% relative to their respective speeds.

In the second case, when two of the spheres, say A and C, are close to each other while the third one, say B, is far away, we first expressed the disturbance of the fluid velocity field $\boldsymbol{u}$ at a point $\boldsymbol{x}$ due to the presence of B as

$$\boldsymbol{u}=\boldsymbol{F}(\boldsymbol{r}):\boldsymbol{E}, \tag{16}$$

where $\boldsymbol{r}=\boldsymbol{x}-\boldsymbol{Y}$. The above was then expanded about the midpoint of A and C as

$$\boldsymbol{u}(\boldsymbol{x})=\boldsymbol{u}(\boldsymbol{x}_0)+\boldsymbol{E}'\cdot(\boldsymbol{x}-\boldsymbol{x}_0)+\tfrac{1}{2}\boldsymbol{\Omega}'\times(\boldsymbol{x}-\boldsymbol{x}_0)+..., \tag{17}$$

where $\boldsymbol{x}_0=(\boldsymbol{X}+\boldsymbol{Z})/2$, (see figure 1), while

$$\boldsymbol{\Omega}'=\tfrac{1}{2}\nabla\times\boldsymbol{u}|_{x_0},\quad \boldsymbol{E}'=\tfrac{1}{2}[\nabla\boldsymbol{u}+(\nabla\boldsymbol{u})^T]|_{x_0}. \tag{18}$$

Accordingly, up to and including terms of $O(1/r^3)$, A and C can be viewed as being immersed in a linear flow field with rate-of-strain tensor $\boldsymbol{E}+\boldsymbol{E}'$ and angular velocity of solid-body rotation $\boldsymbol{\Omega}+\boldsymbol{\Omega}'$, so that the velocities of A and C are given by

$$\boldsymbol{V}^{(A)}=\boldsymbol{U}(\boldsymbol{x}_0)+\boldsymbol{u}(\boldsymbol{x}_0-\boldsymbol{Y})-\tfrac{1}{2}\boldsymbol{r}'''\cdot(\boldsymbol{E}+\boldsymbol{E}')\cdot[A(r''')\boldsymbol{r}'''\boldsymbol{r}'''/r'''^2+B(r''')(\boldsymbol{I}-\boldsymbol{r}'''\boldsymbol{r}'''/r'''^2)]$$
$$+\tfrac{1}{2}(\boldsymbol{\Omega}+\boldsymbol{\Omega}')\times\boldsymbol{r}''', \tag{19}$$

and

$$\boldsymbol{V}^{(C)}=\boldsymbol{U}(\boldsymbol{x}_0)+\boldsymbol{u}(\boldsymbol{x}_0-\boldsymbol{Y})+\tfrac{1}{2}\boldsymbol{r}'''\cdot(\boldsymbol{E}+\boldsymbol{E}')\cdot[A(r''')\boldsymbol{r}'''\boldsymbol{r}'''/r'''^2+B(r''')(\boldsymbol{I}-\boldsymbol{r}'''\boldsymbol{r}'''/r'''^2)]$$
$$-\tfrac{1}{2}(\boldsymbol{\Omega}+\boldsymbol{\Omega}')\times\boldsymbol{r}''', \tag{20}$$

where the functions $A(r)$ and $B(r)$ are given by Batchelor & Green (1972*a*). The accuracy of (19) and (20) is discussed in the next section.

Finally, the velocity of B can be evaluated by assuming pairwise additivity, i.e. by neglecting the effect on B of the reflections between A and C.

An important property of equations (19) and (20) is that, by providing the correct expression for the relative velocities of spheres A and C when they are close to each

other, we prevent these two particles from ever overlapping during the course of the numerical calculation of their trajectories.

Finally, when all three spheres are close together, pairwise additivity was used to determine the velocities of the spheres. Despite its being a crude approximation, this assumption did not affect the final result of our computation by more than 2%, as discussed in the next Section.

5. The lateral displacement resulting from an encounter

The lateral displacement of a fluid point resulting from its encounter with two incoming spheres can be obtained by integrating the equations for the trajectories

$$\frac{dX}{dt} = V^{(A^*)}, \quad \frac{dY}{dt} = V^{(B)}, \quad \frac{dZ}{dt} = V^{(C)}, \tag{21}$$

together with the initial positions of the spheres at time $t = 0$.

Let us start by considering the case when the three objects do not get too close to one another during their encounter, so that the reflection result (14) can be used to determine their trajectories. In this case, an asymptotic expression for ΔX_j is obtained by the method of successive approximations as

$$\Delta X_j = \int V_j^{(A^*)}(\xi)dt \tag{22}$$

with $\xi = (X, Y, Z)$ given by

$$\xi = \int V dt \tag{23}$$

and $V = (V^{(A^*)}, V^{(B)}, V^{(C)})$, where V and ξ are expanded as $V = V^{(0)} + V^{(1)} + V^{(2)} + \ldots$ and $\xi = \xi^{(0)} + \xi^{(1)} + \xi^{(2)} + \ldots$ with $V^{(0)}$, $V^{(1)}$ etc. denoting the successive terms of different order in $1/\bar{r}$ in (14). At zeroth order, all interactions between the spheres and the fluid particle are neglected, i.e. $V^{(0)} = U$, so that the trajectories are just the unperturbed streamlines, with no lateral displacement. Next, considering that $V^{(1)} \sim O(1/\bar{r}^2)$ and $V^{(2)} \sim O(1/\bar{r}^4)$, where $\bar{r}$ is the typical distance between the spheres during their encounter, we find that again $\Delta X_j = 0$ due to the left–right symmetry of $V^{(1)}(\xi^{(0)})$ and $V^{(2)}(\xi^{(0)})$.

Therefore, the leading term in the lateral displacement ΔX_j is $O(1/\bar{r}^5)$ and is due to both $V^{(1)}(\xi^{(0)} + \xi^{(1)})$ and $V^{(3)}(\xi^{(0)})$.

Comparison of the $O(1/\bar{r}^5)$ leading term of the lateral displacement ΔX_j, as obtained from this asymptotic analysis, with the results of direct numerical integration showed excellent agreement for all initial configurations of the spheres as long as the distances between any two spheres and those between the fluid particle and the spheres were $O(1)$ or larger.

For the case where the three objects are not always far apart from one another, equations (21) were integrated numerically using a fourth-order Runge–Kutta scheme.

A similar approach was used to determine the lateral displacement of a test sphere. In particular, the method of successive approximations can also be used to determine the lateral displacement of the test sphere with the result that the leading term in the far-field asymptotic form is found to be also of $O(1/\bar{r}^5)$. As an example, we plot, in figure 3, the displacement of A due to an encounter such that the trajectories of A, B and C pass through the points $(0, 0, 0)$, $(0, 3d, 4d)$ and $(2d, 2d, 2d)$ respectively, where

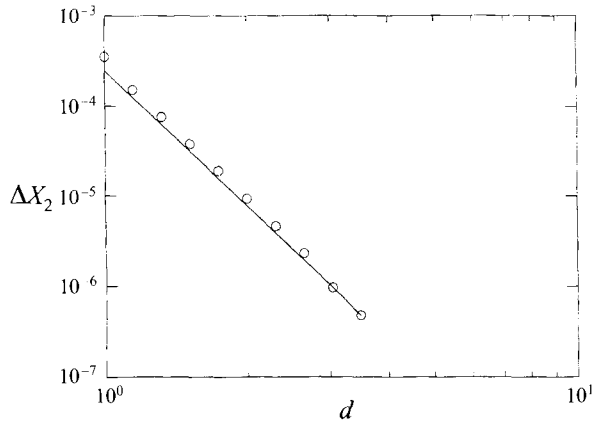

FIGURE 3. Displacement ΔX_2 of the test sphere due to encounters, when A, B and C pass through the points (0, 0, 0), (0, 3*d*, 4*d*) and (2*d*, 2*d*, 2*d*), respectively, as a function of *d*. ○, Numerical results; —, asymptotic results using the far-field expansion as described following (15).

$d \geqslant 1$. It is seen that the agreement between the two sets of calculations is excellent even when the distances between the three objects during their encounter are of $O(1)$.

The numerical results for the displacement ΔX_j using the far-field expansion (13) for the velocity of the particles and those obtained by truncating the expansion to $O(1/r^5)$ were also compared and were found to differ by less than 5%. The difference could be positive or negative depending on the initial configurations. Specifically, for the trajectory passing through the configuration A(0,0,0), B(−3,1.5,0) and C(−6,2,0), ΔX_2 increased by 4% if the expansion (13) was truncated at $O(1/\bar{r}^5)$.

At this point, a brief discussion is in order about the time step used to determine the particle trajectories. First of all, in addition to using a base time step, we also used a smaller one (i.e. one fifth of the base time step) when the three objects were close ($\bar{r} < 3$) and a larger one (i.e. four times the base time step) when they were far apart ($\bar{r} > 20$). In addition, in order to determine the value of the base time step, we studied the trajectories of a closed pair of spheres and showed that when the base time step equalled 0.2, the spheres returned to their initial positions to within a 10^{-2} approximation after completing 10 revolutions. Therefore, as the times involved in our collision were always shorter than that of this example, we concluded that 0.2 is a safe choice for our base time step.

In the computation of the net transverse displacement, ΔX_j, of the tracer particle for each given initial configuration of the spheres B and C, we must also calculate the forward and backward particle trajectories, from $t = 0$ to $t = +\infty$ and from $t = 0$ to $t = -\infty$, respectively. Therefore, in our numerical integrations, we defined a cut-off distance L such that, whenever the distance between the tracer and either B or C became larger than L, the effect of this far away sphere could be neglected, while that of the other sphere could easily be accounted for in terms of two-body interactions. But, since ΔX_j is the difference between the forward and backward displacements and is usually much smaller in magnitude than either of them, L must be large enough such that the cut-off error is small not only compared to the forward and backward displacements, but also compared to the net displacement ΔX_j. In fact, L can be estimated in terms of the error ϵ, say, in the net displacement due to interactions that take place outside the cut-off region. Thus, by considering that the transverse velocity component of the test sphere is of $O(1/\bar{r}^3)$ and then integrating outside the cut-off

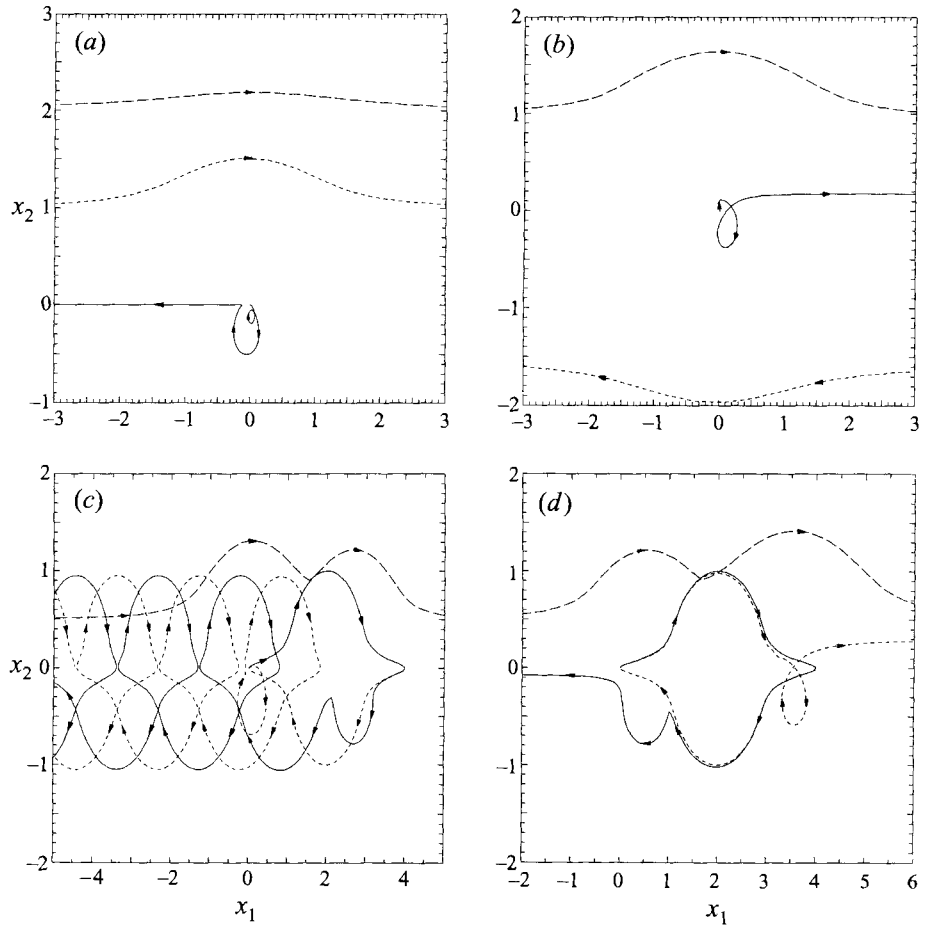

FIGURE 4. Typical trajectories of spheres A (—), B (— — —) and C (- - - - - -), where their centres remain along the plane $x_3 = 0$. (*a*) B and C come from infinity on the same side and interact with A, when $\boldsymbol{X}^{(0)} = (0,0,0)$, $\boldsymbol{Y}^{(0)} = (-30,2,0)$ and $\boldsymbol{Z}^{(0)} = (-20,1,0)$; (*b*) B and C come from infinity on the different sides and interact with A; when $\boldsymbol{X}^{(0)} = (0,0,0)$, $\boldsymbol{Y}^{(0)} = (-30,-1.6,0)$ and $\boldsymbol{Z}^{(0)} = (-20,1,0)$; (*c*) A and C orbit around each other initially and remain bound after interacting with B, when $\boldsymbol{X}^{(0)} = (0,0,0)$, $\boldsymbol{Y}^{(0)} = (-28,0.5,0)$ and $\boldsymbol{Z}^{(0)} = (4,0,0)$; (*d*) A and C orbit around each other initially and break up after interacting with B, when $\boldsymbol{X}^{(0)} = (0,0,0)$, $\boldsymbol{Y}^{(0)} = (-33,0.5,0)$ and $\boldsymbol{Z}^{(0)} = (4,0,0)$.

region, we found that $L \sim O(1/\epsilon^{1/2})$. This point will be discussed further in detail in §6.2.

A few typical trajectories are plotted in figure 4, where the centres of all three spheres remain within the plane $x_3 = 0$. In particular, we wish to note that a bound pair of spheres was found to break up as a result of its interaction with a third sphere only very rarely, which is consistent with the fact that this can happen only when the relative positions of the spheres comprising the doublet are displaced out of the region of closed trajectories. Also, we observed that even in the most extreme cases, no particle overlapping occurred during the computation of the particle trajectories, thereby confirming that (19) and (20) indeed account for the correct lubrication force among the spheres.

To better illustrate the salient features of these encounters, $(\Delta X_2)^2$ is plotted

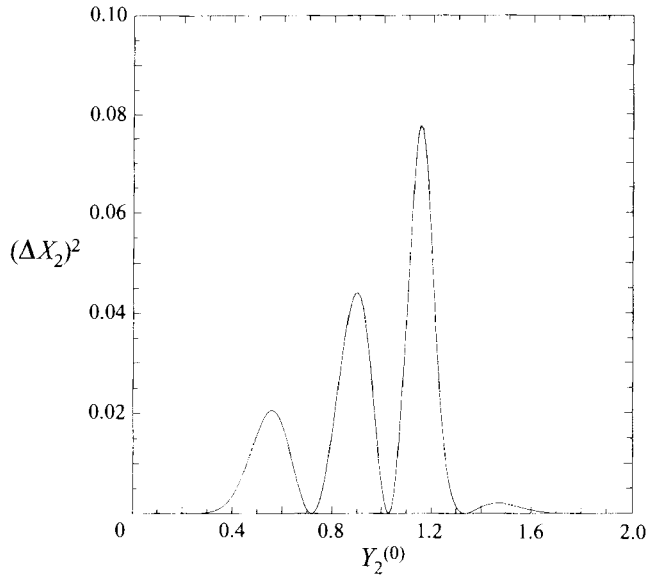

FIGURE 5. An illustration of the dependence of $(\Delta X_2)^2$ on Y_2, assuming that the initial configuration of A*, B and C is $\boldsymbol{X}^{(0)} = (0,0,0)$, $\boldsymbol{Y}^{(0)} = (-3, Y_2, 0)$ and $\boldsymbol{Z}^{(0)} = (-6,2,0)$, respectively.

as a function of $Y_2^{(0)}$ in figure 5 for the initial configuration $\boldsymbol{X}^{(0)} = (0,0,0)$, $\boldsymbol{Y}^{(0)} = (-3, Y_2^{(0)}, 0)$ and $\boldsymbol{Z}^{(0)} = (-6,2,0)$. The existence of several peaks and zeros in this curve is a general feature of the integrand in the expressions for the diffusion coefficients, which greatly increased the difficulty in obtaining accurate numerical values for the corresponding integrals. The zeros correspond to these initial configurations, for which the trajectories of A, B and C are symmetric with respect to a plane perpendicular to the $\boldsymbol{e}_1$-axis. For example, in the case where A, B and C happen to lie on the same plane perpendicular to the $\boldsymbol{e}_1$-axis at a certain instant of time, the trajectories of A, B and C are then symmetric with respect to that plane, owing to the reversibility of the Stokes equations, and hence such encounters do not lead to a net lateral displacement of A. As another example, when B and C happen to lie on the same line parallel to the $\boldsymbol{e}_1$-axis while A lies on the plane passing through the midpoint of B and C and perpendicular to the $\boldsymbol{e}_1$-axis, then the trajectories are again symmetric with a zero lateral net displacement for A.

6. The determination of the diffusion coefficients

Finally, we turn to the task of calculating the integrals (3), (4), (7), (8) and their counterparts for the particle diffusivities, and thereby determine all the diffusion coefficients defined in §2. Before doing this, we wish to show, however, that the integrals converge as the size of the collision box $l \longrightarrow \infty$, so that they can be evaluated using a large but finite collision box without having to resort to a renormalization.

6.1. *The convergency of the integrals*

First, let us consider the integral (3) when all the variables $Y_2^{(0)}, Y_3^{(0)}, Z_1^{(0)}, Z_2^{(0)}$ and $Z_3^{(0)}$ together with r_{BC} are of $O(\bar{r})$, where $\bar{r} \gg 1$. In this case, we have seen (see §4) that ΔX_j is of $O(1/\bar{r}^5)$, so that the integral in (3) converges as the size of the collision box $l \longrightarrow \infty$, and the error, i.e. the neglected contribution from encounters that take

place outside the collision box, is of $O(1/l^4)$. Another contribution to the integral in (3) comes from the case where $Y_2^{(0)}$ and $Y_3^{(0)}$ are of $O(1)$, while the variables $Z_1^{(0)}, Z_2^{(0)}$ and $Z_3^{(0)}$ are of $O(\bar{r})$, with $\bar{r} \gg 1$. Here, since B is moving slowly near the x_1-axis, the leading-order effect of C on $V^{(A^*)}$ is the $O(1/\bar{r}^2)$-term disturbance in the far-field expansion, which, however, does not contribute directly to the lateral displacement of A*, due to its left-right symmetry. But, this disturbance is reflected by B to A* and contributes an $O(1/\bar{r}^3)$-term to ΔX_j. So, this contribution to the integrand of (3) is of $O(1/\bar{r}^6)$ and its integral converges as the size of the collision box $l \longrightarrow \infty$, with the error vanishing as $1/l^3$. A similar result is obtained when $Y_2^{(0)}$ and $Y_3^{(0)}$ are of $O(\bar{r})$, while $r_{BC} \sim O(1)$, that is when B and C are close to each other and far from the e_1-axis.

The integral (4) can be considered in the same way. Here, since $Z_1^{(0)}, Z_2^{(0)}$ and $Z_3^{(0)}$ are of $O(1)$, while $Y_1^{(0)}$ and $Y_2^{(0)}$ are of $O(\bar{r})$, the displacement ΔX_j is of $O(1/\bar{r}^3)$, the integrand in (4) is of $O(1/\bar{r}^5)$ and the integral converges as $l \longrightarrow \infty$, with the error vanishing as $1/l^3$.

Since, obviously, the integrals (7) and (8) converge even faster than (3) and (4), respectively, we can safely conclude that the fluid transverse diffusivities are determined via a series of integrals that converge as the dimension of the collision box $l \longrightarrow \infty$. The same arguments can be applied to the corresponding expressions for the particle diffusivities.

Finally, as described below, all the integrals were evaluated numerically over the domains discussed in §2 by applying a Gaussian-type scheme in order to minimize the number of trajectories that had to be computed.

6.2. *The monolayer fluid and particle diffusivities*

We started by computing the integral (7) for the monolayer diffusivity of the fluid tracer A*, which requires less computational time, so that we could easily study the consequences of the various changes of the computational parameters such as the number of mesh points needed in evaluating the integrals, the time step for the trajectory integration, the size of the box l and the cut-off distance L.

As was described in §2, the integral (7) was evaluated fold by fold with respect to, in sequence, $Z_1^{(0)}, Z_2^{(0)}$ and $Y_2^{(0)}$. The first fold integration, i.e. that with respect to $Z_1^{(0)}$, was performed for different fixed values of $Z_2^{(0)}$ at a given $Y_2^{(0)}$ and with different numbers of mesh points, using a six-point Gaussian quadrature and taking into account that the integrand has several peaks and zeros, as mentioned in §6.1 (see figure 5). In order to quantify the sensitivity of the integral to the number of mesh points, we compared the values of the integral as obtained using 24 and 48 mesh points, and found that the difference between the two sets was within 1% in this typical case.

Concerning the integration with respect to $Z_2^{(0)}$, it turned out, again, that the difference between using 24 mesh points and 48 mesh points was within 1%. In addition, it appeared that most of the contribution to the final fold of integration, i.e. that with respect to $Y_2^{(0)}$, comes from the interval $0 < Y_2^{(0)} < 1.5$ and that the integrand has only one peak with respect to $Y_2^{(0)}$. Therefore, we integrated with respect to $Y_2^{(0)}$ by distributing 12 mesh points in the interval $0 < Y_2^{(0)} < 1.5$ and 6 in the interval $1.5 < Y_2^{(0)} < 4$, and then verified that the results of the integration were within 1% of those obtained using twice as many mesh points.

Now, we turn to the values of l and L. The size of the box l was set equal to 4; a decrease from 4 to 3.5 was found to alter the final result by only 0.3%. For the cut-off

distance L, we used $L = 2000$, and verified that the results of the integration were within 1% of those obtained using $L = 1000$. On the other hand, when $L < 100$, the results strongly depend on L. A simple estimate can help to explain why L must be so large. Since the error in the diffusion coefficient resulting from a small uncertainty ϵ, say, in the net lateral displacement of the tracer is $O(\epsilon l^4)$, by requiring that this error must be less than 1%, we find that $\epsilon \sim O(10^{-6})$. Therefore since L is proportional to $1/\epsilon^{1/2}$ (see §5), we find that $L \sim O(10^3)$, in agreement with our numerical estimate.

Similarly, we evaluated the integral (8) and obtained for the monolayer diffusivity of a fluid tracer $\bar{D}_2^* = 0.067\bar{c}^2$.

As a further check of the above result, we doubled the number of all the mesh points used in the three folds of our integrations and found that the first two significant digits in the coefficient of diffusivity remained unchanged. In addition, an increase of the basic time step from 0.2 to 0.4 was found to alter the final result by less than 0.1%.

In the computations referred above, we assumed that the expression for $\bar{p}(\boldsymbol{r})$ is valid both outside and inside the region of closed trajectories, corresponding to the case where a well-mixed suspension is first sheared in a pure straining flow and then is subjected to a simple shear flow. On comparing this value of $\bar{D}_2^*$ with that obtained by letting $\bar{p}(\boldsymbol{r}) = 1$ (i.e. a well-mixed suspension) within the region of closed streamlines, we found that the two results were only 0.2% apart, thereby showing that the value of $\bar{D}_2^*$ is insensitive to the choice of the pair distribution function within the region of closed trajectories.

We now turn to the monolayer diffusivity of a test sphere. As we discussed in §4, this case is fundamentally different from that of the fluid diffusivity since, unlike the fluid velocity, which is known exactly, the velocity of a test sphere in the vicinity of two other spheres is known only approximately. First, let us examine the case when either B or C is close to A, while the other sphere is far away. Here, the sphere velocity can be determined approximately using (19) together with the conditions of pairwise additivity applied to the far away particles. In order to test the accuracy of this approximation, we derived similar equations for the velocity of a fluid particle in the vicinity of two spheres and compared the values of the fluid diffusivity $\bar{D}_2^*$, as obtained using this approximate expression, with that using Lamb's 100-term series expansion, finding that the two results were within 1% of each other. Hence, we concluded that (19) can be safely used to determine the lateral displacement of the test particle in the vicinity of one of the other spheres.

Next, let us consider the case where, at some time during their encounter, the three spheres are in close proximity with each other. Here, a simple estimate shows that the contribution to the particle diffusivity due to those initial configurations which lead to such close encounters, is of $O[\epsilon^{0.6}(\Delta X_j)^2]$, where ϵ is the gap between any two close particles while ΔX_j is the typical net lateral displacement resulting from such close encounters. (Here, we have assumed that the pair conditional probability diverges as $\epsilon^{-0.8}$ (Batchelor & Green, 1972*b*).) Therefore, since both ϵ and ΔX_j are of $O(10^{-1})$, we conclude that the error in the diffusion coefficient is less than 1%, even when the tracer velocity is evaluated to an accuracy of $\pm 20\%$, which grossly over-estimates the error introduced by using (19) for such close encounters. As a double check, we also computed numerically the contribution to the diffusivity of the close encounters, finding that it is about 5%, thereby confirming the above estimate.

Finally, we computed the particle monolayer diffusivity for a test sphere using the same number of mesh points, box length, cut-off distance and base time step as for the computation of the liquid monolayer diffusivity and found that $\bar{D}_2 = 0.032\bar{c}^2$.

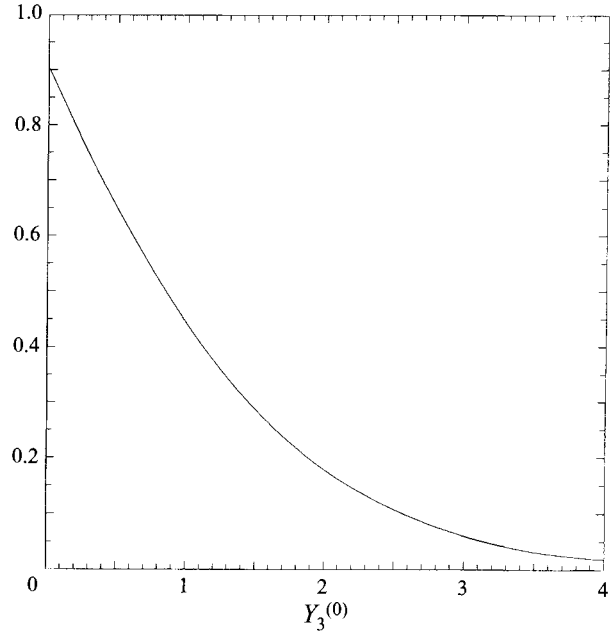

FIGURE 6. An illustration of the dependence of the integrand on $Y_3^{(0)}$ after the first three fold integrations with respect to $Z_1^{(0)}$, $Z_2^{(0)}$ and $Y_2^{(0)}$ have been performed and keeping $Z_3^{(0)} = 0$.

Particle monolayer diffusivities, as obtained by direct numerical simulations, have been reported by Bossis & Brady (1987) for $\bar{c} = 0.453$ and by Chang & Powell (1994) for $0.12 \leqslant \bar{c} \leqslant 0.60$. Although these values of $\bar{c}$ are of course quite outside the range of our analysis, Chang & Powell (1994) reported that, for $\bar{c} \leqslant 0.25$, $\bar{D}_2$, was found to scale as $\bar{c}^2$ with the constant of proportionality being approximately 0.2, i.e. six times greater than the value 0.032 that resulted from our analysis. One possible reason for this discrepancy may be due the the fact that, in the direct simulations of Chang & Powell (1994) using periodic boundary conditions, all interactions between a particle located at the centre of a unit cell and the particles outside the periodic cell were neglected, with the distance between the centre of the cell and its outer edge being approximately 15. But, when we recomputed $\bar{D}_2$ using our analysis by deliberately neglecting all interactions between any two particles whenever their separation exceeded 15, the coefficient was found to increase by a factor of 4. Thus, it would appear that, at least for very dilute systems, the cut-off distance used for far-field interactions, and therefore the size of the periodic box in numerical simulations, must be quite large. This point, though, deserves further study.

6.3. *The fluid and particle diffusivities*

The evaluation of (3) and (4) is almost the same as that of (7) and (8), except that it is more computationally intensive because of the additional two fold integrations which need to be performed. The plot of the integrand in (3) for the last two fold integrations is shown in figure 6 as a function of $Y_3^{(0)}$ for fixed $Z_3^{(0)} = 0$. The curve appears to be smooth, decreasing monotonically with respect to $Y_3^{(0)}$ and the major contribution to the integral comes from the region $Y_3^{(0)} < 2$. Using 12 mesh points

for the last two fold integrations, we found for the liquid diffusivities $D_2^* = 0.12c^2$ and $D_3^* = 0.004c^2$.

Finally, the diffusivity of a test sphere was computed in the same way, giving $D_2 = 0.11c^2$ and $D_3 = 0.005c^2$.

It is surprising that for both the liquid and the particle diffusivities, the diffusion coefficient in the vorticity or e_3-direction is smaller than that in the direction of the plane of shear, or e_2 direction, by a factor of about 20. This is consistent with the corresponding results of da Cunha & Hinch (1996) for the self-diffusivities due to particles roughness, who obtained a corresponding ratio of about 10. Both these results, however, are limited to very dilute suspensions. In contrast, Phan & Leighton (1996) reported from experimental observations that this ratio for the particle diffusivities equals approximately 2/3 when $0.30 < c < 0.55$.

Recently, Biemfohr *et al.* (1996) measured experimentally the effective shear-induced coefficient of self-diffusion in a suspension of monodisperse spheres, finding that, in the dilute limit, the leading-order term is of $O(c)$. Clearly, this result cannot apply to perfect spheres and can only be attributed to the non-sphericity and/or roughness of the particles that were employed. As for the coefficient of the next, $O(c^2)$, term, their measurements indicated that it is very small, consistent with our findings.

This work was supported in part by the National Science Foundation grant CTS-9318820 and by the State of New York under its Einstein Chair Program.

REFERENCES

ACRIVOS, A., BATCHELOR, G. K., HINCH, E. J., KOCH, D. L. & MAURI, R. 1992 Longitudinal shear-induced diffusion of spheres in a dilute suspension. *J. Fluid Mech.* **240**, 651.

BATCHELOR, G. K. & GREEN, J. T. 1972*a* The hydrodynamic interaction of two small freely-moving spheres in a linear flow field. *J. Fluid Mech.* **56**, 375.

BATCHELOR, G. K. & GREEN, J. T. 1972*b* The determination of the bulk stress in a suspension of spherical particles to order c^2. *J. Fluid Mech.* **56**, 400.

BIEMFOHR, S., LOOBY, T., BIEMFOHR, S. & LEIGHTON, D. 1996 Measurement of the shear-induced coefficient of self-diffusion in dilute suspensions. *J. Fluid Mech.* (submitted).

BOSSIS, G. & BRADY, J. F. 1987 Self-diffusion of Brownian particles in concentrated suspensions under shear. *J. Chem. Phys.* **87**, 5437.

CHANG, C. & POWELL, R. L. 1994 Self-diffusion of bimodal suspensions of hydrodynamically interacting spherical particles in shearing flow. *J. Fluid Mech.* **281**, 51.

CICHOCKI, B., FELDERHOF, B. U., HINSEN, K., WAJNRYB, E. & BLAWZDZIEWICZ, J. 1994 Friction and mobility of many spheres in Stokes flow. *J. Chem. Phys.* **100**, 3780.

CUNHA, F. R. DA & HINCH, E. J. 1996 Shear-induced dispersion in a dilute suspension of rough spheres. *J. Fluid Mech.* **309**, 211.

ECKSTEIN, E. C., BAILEY, D. G. & SHAPIRO, A. H. 1977 Self-diffusion of particles in shear flow of a suspension. *J. Fluid Mech.* **79**, 191.

HASSONJEE, Q., PFEFFER, R. & GANATOS, P. 1992 Behavior of multiple spheres in shear and Poiseuille flow fields at low Reynolds number. *Int. J. Multiphase Flow* **18**, 353.

KIM, S. 1987 Stokes flow past three spheres: An analytic solution. *Phys. Fluids* **30**, 2309.

KIM, S. & KARRILA, S. J. 1991 *Microhydrodynamics: Principles and Selected Applications.* Butterworth-Heinemann.

LEIGHTON, D. & ACRIVOS, A. 1987*a* Measurement of shear-induced self-diffusion in concentrated suspensions of spheres. *J. Fluid Mech.* **177**, 109.

LEIGHTON, D. & ACRIVOS, A. 1987*b* The shear-induced migration of particles in concentrated suspensions. *J. Fluid Mech.* **181**, 415.

MAZUR, P. & VAN SAARLOOS, W. 1982 Many-sphere hydrodynamic interactions and mobilities in a suspension. *Physica A* **115**, 21.

PHAN, S. E. & LEIGHTON, D. 1996 Measurement of the shear-induced tracer diffusivity in concentrated suspensions. *J. Fluid Mech.* (submitted).

VAN SAARLOOS, W. & MAZUR, P. 1983 Many-sphere hydrodynamic interactions II. Mobilities at finite frequencies. *Physica* A **120**, 77.

YOON, B. J. & KIM, S. 1987 Note on the direct calculation of mobility functions for two equal-sized spheres in Stokes flow. *J. Fluid Mech.* **185**, 437.